Available online at www.sciencedirect.com

ScienceDirect

Ceramics International 41 (2015) 2367–2372

CERAMICS INTERNATIONAL

www.elsevier.com/locate/ceramint

Magneto-electric coupling study in multiferroic $La_{0.7}Ba_{0.3}MnO_3$–$BaTiO_3$ composite ceramic at room temperature

Ling Zhou[a], Qiuyun Fu[a,*], Dongxiang Zhou[a], Fei Xue[a], Yahui Tian[a], Liangbin Hao[b]

[a]School of Optical and Electronic Information, Huazhong University of Science and Technology, Wuhan 430074, People's Republic of China
[b]Beijing Aerospace Times Optical-Electronic Technology Co., Ltd., Beijing 100094, People's Republic of China

Received 29 July 2014; received in revised form 8 October 2014; accepted 8 October 2014
Available online 16 October 2014

Abstract

A multiferroic $La_{0.7}Ba_{0.3}MnO_3$–$BaTiO_3$ composite sample was prepared by the solid state method. The composite exhibits a ferroelectric feature (2Pr = 10.52 μC/cm^2, 2Ec = 32.2 kV/cm) and weak ferromagnetic feature (2Mr = 13.6 memu/g, 2Hc = 60.5 Oe). More importantly magneto-electric coupling, as well as magneto-capacitance and magneto-impedance effects, was also observed. The average changes of the 2Pr and 2Ec were −21.1% and −9.2%, respectively, when a relatively low external magnetic field (H = 200 Oe) was applied. The MC value was ~ −1.9% at 1 MHz after the sample was magnetized. These ME effects were mainly originated from the coexistence of magnetostriction and magneto-resistance in LBMO.

Keywords: B. Composite; $La_{0.7}Ba_{0.3}MnO_3$; $BaTiO_3$; Magneto-electric coupling

1. Introduction

In recent years, multiferroic/magneto-electric (ME) materials have attracted great interest because of their potential applications in four-state logic memory devices, magneto-electric random access memory and magneto-electric sensors [1–3]. However, it is still a significant challenge to find proper materials with both multiferroic order and significant ME coupling at room temperature. Due to weak ME coupling at and above room temperatures in single-phase materials, increasing interest has been focused on composite multiferroics. Composite multiferroics can be labeled according to their architectures, such as particulate-based composites (0–3) [4–8], layered heterostructures (2–2) [9–12], pillars within a 3-D matrix (1–3) [13–14], and core–shell structures [15–17]. Compared with the weak mechanical coupling in 2–2 structures and difficulty in implementation of 1–3 and core–shell structures, particulate-based composites still attracted great attention because of their relative large mechanical coupling, superior mechanical strength and ease of fabrication. Many researchers have reported 0–3 bulk composites consisting of perovskite structured $BaTiO_3$ (BTO) or $Pb(Zr_{0.52}Ti_{0.48})O_3$ (PZT) and spinel structured AFe_2O_4 (A=Co, Ni and Zn) for their outstanding piezoelectricity and good magnetostriction, respectively. However, the bulk composites with the same structure are rarely mentioned.

Cai-Xia Li [7] group has synthesized $0.33Ba_{0.70}Ca_{0.30}TiO_3$–$0.67BiFeO_3$ diphasic ceramics with two perovskite structures. The ceramics exhibit the magneto-capacitance effect, which is defined as the relative change of the dielectric constant as a function of the applied magnetic field and expressed as $((\varepsilon_r(H)-\varepsilon_r(0))/\varepsilon_r(0))$. The magneto-capacitance coefficient was 2.96% when the applied magnetic fields changed from 0 Oe to 10 kOe. The group of N.G. Kim [8] investigated the magneto-capacitance effect in $BaTiO_3-LaMnO_3$ composites; the value $((\varepsilon(H)-\varepsilon(0))/\varepsilon\ (0))$ of all samples is quite small ($<1\%$), even in strong magnetic field with 9 T. The authors mentioned that the phase formation of (La,Ba)MnO_3 was

*Corresponding author. Tel.: +86 27 87558482, +86 18602717211; fax : +86 27 87558482.
E-mail address: fuqy@mail.hust.edu.cn (Q. Fu).

http://dx.doi.org/10.1016/j.ceramint.2014.10.049
0272-8842/

crucial for magneto-capacitance effect. The origin of such effect was due to the coexistence of magneto-resistance and magnetostriction in (La,Ba)MnO_3. However, for the above diphasic ceramics with the two perovskites structure, the magneto-capacitive effects are relatively weak. This may be due to the antiferromagnetic features of $BiFeO_3$ and $LaMnO_3$, as well as their small magnetostriction coefficient. Therefore, in this work, we attempted to prepare composite ceramics with two perovskites structures consisting of excellent ferro electric material and strong ferromagnetic material with large magnetostriction coefficient to achieve better multiferroic and magneto-electric effects.

BTO is an excellent ferroelectric material, which is widely used as piezoelectric transducers, high permittivity capacitors and infrared detectors [18]. The theoretical saturation polarization (P_s) is 20.35 μC/cm^2, and the piezoelectric constant d_{33} is 460 pC/N. $La_{0.7}Ba_{0.3}MnO_3$ (LBMO), as mentioned above, is a ferromagnetic material; the saturation magnetization (Ms) is ~80 emu/g (T=5 K), and the curie temperature (Tc) is ~290 K [19,20]. Moreover, LBMO has an outstanding magnetostriction property at room temperature, achieving 254×10^{-6} in a magnetic field of 8.2 kOe [21]. The value is greater than the saturation magnetostriction coefficients of $NiFe_2O_4$, $Co_{0.8}Zn_{0.2}Fe_2O_4$ and $CoFe_2O_4$, which are approximately -26×10^{-6}, -98×10^{-6}, and -105×10^{-6} [22], respectively. In this work, we prepared a LBMO–BTO composite ceramic using the solid state method. The structureal, ferroelectric, leakage current, magnetic and magneto-electric properties are discussed in detail.

2. Experimental

The LBMO–BTO ceramics were fabricated by the conventional solid-state reaction method. The synthesis of LBMO was performed using the solid-state reaction method. Analytical-grade raw materials $KMnO_4$ and $MnCl_2\cdot4H_2O$ were mixed and ground in an agate mortar for 30 min, and then mixed with $BaCl_2$ and La_2O_3 (99.99%) and ground with ethanol for 2 h. The mixture was dried at 70 °C, calcined at 1200 °C for 4 h in air and slowly cooled to RT in the furnace. The BTO powder was prepared using the sol–gel method. The synthesis followed our previous work [10], while the gel (Ba:Ti=1:1) was dried and calcined in air at 800 °C for 2 h. Subsequently, LBMO and BTO powders with 0.1:0.9 mass ratios were weighed and ball milled for 4 h with alcohol as the medium. After drying, the mixed powders were pressed into pellets of 1 mm in thickness and 10 mm in diameter at a pressure of 150 MPa, using PVA as a binder. After burning off PVA at 550 °C for 30 min, the pellets were finally sintered at 1300 °C for 2 h in air. The samples were burnished and pasted with silver on both sides for electric testing. The crystalline phases of the ceramic were probed by a Bruker D8 ADVANCE X-ray diffractometer (XRD) using Cu Kα radiation. The morphology of the composite was verified by a VEGA SBU OXFORD INCA-X-MAX-2C scanning electron microscope (SEM). The polarization–electric field (P–E) hysteresis was tested at room temperature (RT) using a Precision Ferroelectric Tester system by Radiant Technologies, Inc. The magnetic studies were performed using a Lakeshore 7400 vibrating sample magnetometer (VSM). For magneto-electric properties measurement, an external dc magnetic field system was built, as reported in the literature [23]. The external dc magnetic field (H=200 Oe) was tested using a Gaussmeter (LakeShore 475 DSP Gaussmeter). The dielectric permittivity and complex impedance spectrum over the range 10^2–10^6 Hz were measured using an impedance analyzer (HP4294A, Agilent, USA) at RT.

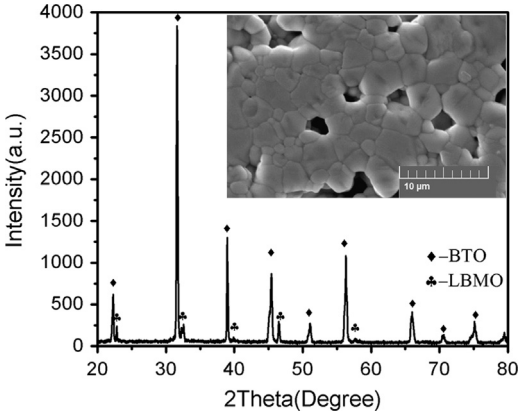

Fig. 1. X-ray diffractograms of LBMO–BTO composite ceramic sintered at 1300 °C. The inset shows the SEM micrograph of the sample.

3. Results and discussion

Fig. 1 shows the XRD patterns for LBMO–BTO ceramics. The XRD patterns indicated that there were two perovskite phases corresponding to tetragonal BTO (JCPDS no. 01-075-0462) and rhombohedral LBMO (JCPDS no. 01-089-0570). The figure shows that no impurity phases are detected, indicating that there is no reaction between the two precursors. The inset shows the micro-morphology of the sample. The sample was polished and heat-treated using the conventional method. The SEM shows that the microstructure is dense globally but a few scattered micropores are observed, which indicates that there is some porosity in the sample. The micropores mainly result from the poor sintering property of LBMO [20]. Research on porous PZT ceramics indicates that the porosity may decrease the piezoelectric coefficient (d_{33}), dielectric constant (ε_r) and remnant polarization (P_r) of the sample, while it may increase the dielectric loss [24–26]. These micropores may also affect the mechanical coupling efficiency of the piezoelectric–magnetostrictive composites, thus leading to lower magnetic coupling effects.

Fig. 2(a) shows the RT P–E loop of the LBMO–BTO sample; the testing frequency is 10 Hz. Although the applied electric field is not sufficient to saturate the loop, the loop still indicates clear ferroelectricity in the sample. The measured remnant polarization 2Pr is 10.52 μC/cm^2 and the coercive field 2Ec is 32.2 kV/cm at a maximum applied electric field of 45 kV/cm. The inset is the leakage current characteristic of the sample. The leakage current density is 1.78×10^{-5} A/cm^2 under an electric field of 20 kV/cm. Fig. 2(b) shows the magnetic hysteresis loop of LBMO–BTO composite ceramic measured at RT. The sample exhibits a weak

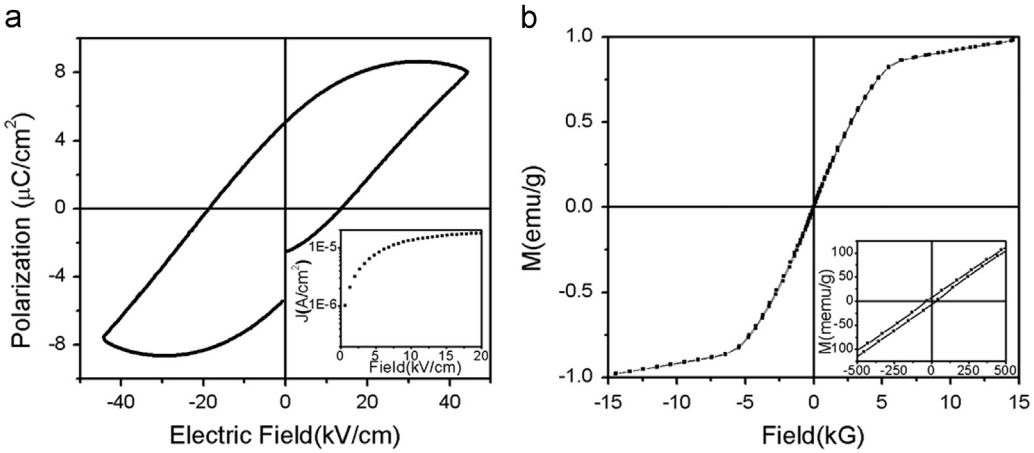

Fig. 2. (a) The *P–E* hysteresis loop of the LBMO–BTO composite ceramic measured at RT. The inset is the leakage current characteristic of the sample and (b) the magnetic hysteresis loop measured at RT.

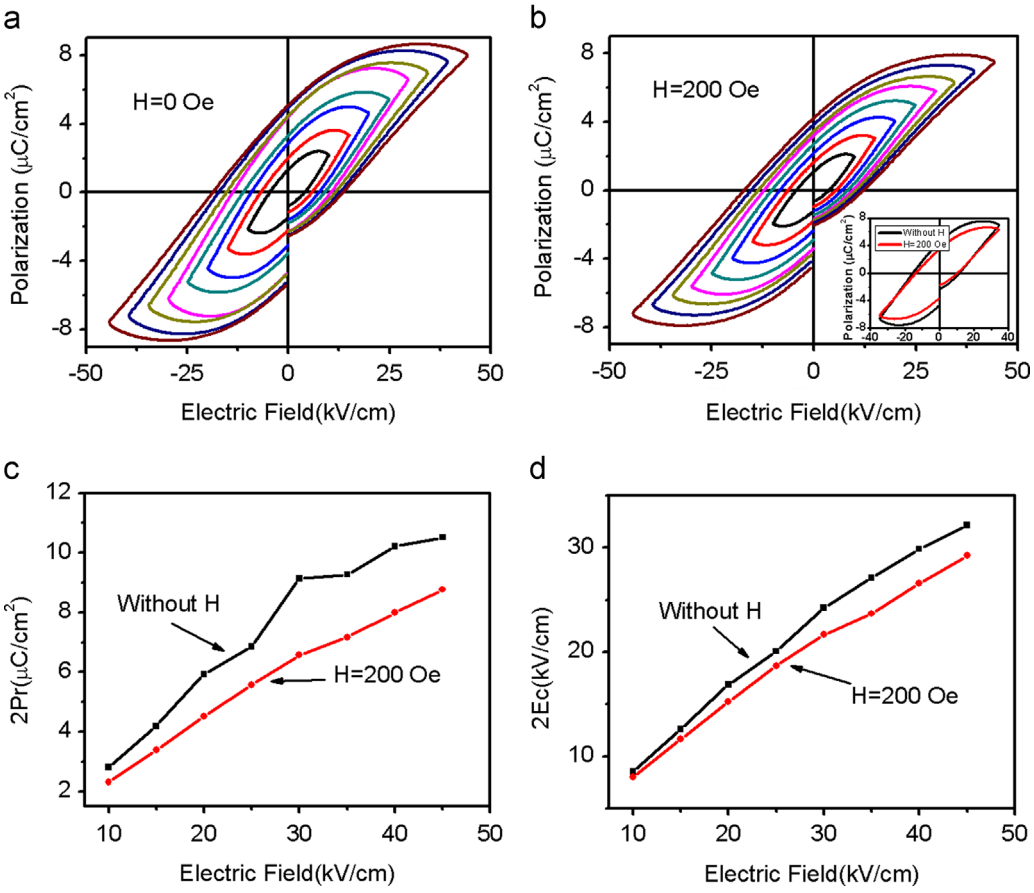

Fig. 3. RT *P–E* hysteresis loops for different values of the maximum electric field E_{max} (a) without and (b) with an external magnetic field *H*. The inset in (b) is the RT *P–E* hysteresis loops measured under the electric field of 35 kV/cm with and without *H*; (c,d) comparison between values of the parameters of (c) remanent polarization 2Pr and (d) coercive field 2Ec as functions of the maximum electric field E_{max} from the *P–E* hysteresis loops in (a) and (b).

ferromagnetic *M–H* loop, with a remnant magnetization (2Mr) of 13.6 memu/g and a coercive field (2Hc) of 60.5 Oe.

The RT ME coupling in LBMO–BTO composite ceramic is demonstrated by the *P–E* hysteresis loops measured without and with an external magnetic field *H*, as often used in the literature [9,15,23]. Fig. 3(a) and (b) shows the RT *P–E* hysteresis loops for different values of the maximum electric field E_{max} without and with an external magnetic field, respectively. The external magnetic field was 200 Oe, which was tested using a gaussmeter. Fig. 3(c) and (d) shows comparisons between values of remnant polarization 2Pr and coercive field 2Ec, respectively, as functions of the maximum electric field E_{max}. It can be seen from the figure that the values of 2Pr and 2Ec decrease when external magnetic field is applied. The average changes of 2Pr and 2Ec are −21.1% and

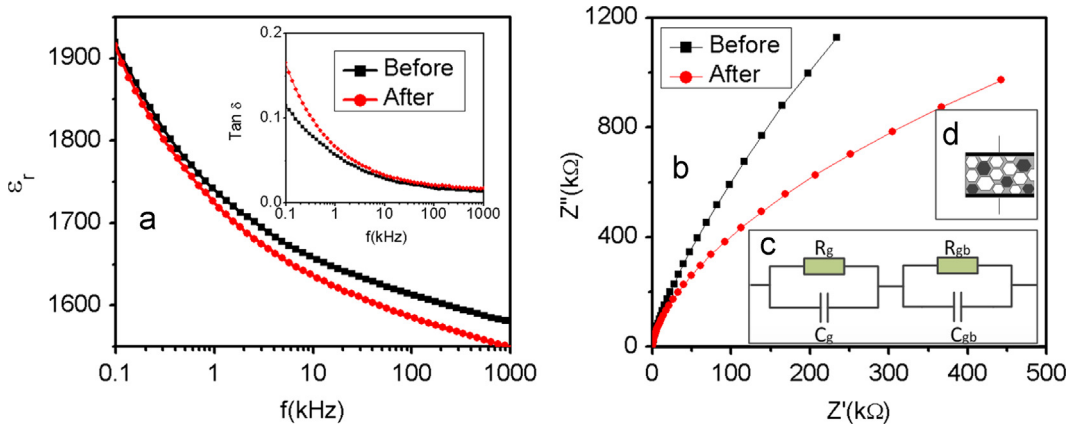

Fig. 4. Frequency dependent behavior of (a) dielectric permittivity (ε_r), where the inset is loss tangent (tan δ); (b) impedance Cole–Cole plots of LBMO–BTO composite before and after being magnetized at RT; (c) the equivalent circuit for the LBMO–BTO composite; and (d) capacitor systems with magneto-resistive Maxwell–Wagner behavior.

−9.2%, respectively, when the magnetic field changes from 0 to 200 Oe. The value is dramatically greater than that of BTO–NFO core–shell composites, which is reported in Ref. [15], in which the maximum change of the remnant polarization is 4.9% with the static magnetic field H increasing from 0 Oe to 2.5 kOe. Therefore, the values suggest that the LBMO–BTO composite ceramic represents strong ME effects even under low static magnetic fields. The ME coupling effects are contributed from the typical mechanism of magnetostrictive–piezoelectric composite materials. The LBMO exhibits positive magnetostriction and stretches with the application of the magnetic field. Thus the BTO will be subjected to a compressive stress across the interface, which leads to the reduction of ferroelectric polarization. As a result, a lower coercive field is necessary to switch fewer domains.

To probe the magneto-capacitance (MC) response we measured the composite's relative dielectric constant ε_r as a function of frequency from 100 Hz to 1 MHz before and after being magnetized, as often reported for other multiferroic materials in the literature. The sample was magnetized in the presence of 3.5 kOe magnetic field for 24 h, and then the ε_r–f measurements were performed, with the sample in the remnant magnetic state. Fig. 4(a) and the inset show the frequency dependence of the dielectric constant and the loss tangent of the composite before and after being magnetized. From the figures we can see that the value of ε_r of the sample is decreased after being magnetized, and the reduction is more obvious in the high-frequency range than in the low-frequency range. The MC value, defined as $MC=[\varepsilon_{(3.5\ kOe)}-\varepsilon_{(0\ Oe)}]\times 100/\varepsilon_{(0\ Oe)}$, is up to $\sim -0.2\%$ at 100 Hz and $\sim -1.9\%$ at 1 MHz. This value is greater than $<0.2\%$ of Mn doped $0.33Ba_{0.70}Ca_{0.30}TiO_3$–$0.67BiFeO_3$ diphasic ceramics at 3 kOe in Ref. [7] and $<1\%$ of $BaTiO_3-LaMnO_3$ composites at 9 T in Ref. [8]. The loss tangent obviously increased after being magnetized, and the increases is more obvious in the low-frequency range than in the high-frequency range. The magneto-loss (ML) value, defined as $ML=[\tan\delta_{(3.5\ kOe)}-\tan\delta_{(0\ Oe)}]\times 100/\tan\delta_{(0\ Oe)}$, is up to ~44.5% at 100 Hz and ~19.9% at 1 MHz.

Impedance spectroscopy of the sample is also performed, with the results presented in the form of Cole–Cole plots, as shown in Fig. 4(b). The Cole–Cole plots are not well-defined semicircles exhibiting a high impedance value of the sample. However, the magneto-impedance (MI) effects are obviously observed. The equivalent circuit for the LBMO–BTO composite could be interpreted as two RC (R: resistant, C: capacitance) circuits in series, as shown in Fig. 4(c). The real part Z' and the imaginary part Z'' of the complex impedance can be obtained from the equation [27,28]

$$Z' = \frac{R_g}{1+(\omega R_g C_g)^2} + \frac{R_{gb}}{1+(\omega R_{gb} C_{gb})^2} \quad (1)$$

$$Z'' = \frac{\omega R_g^2 C_g}{1+(\omega R_g C_g)^2} + \frac{\omega R_{gb}^2 C_{gb}}{1+(\omega R_{gb} C_{gb})^2} \quad (2)$$

where $\omega = 2\pi f$ is the angular frequency, and R_g/C_g and R_{gb}/C_{gb} represent the grain and grain boundary resistances/capacitances, respectively. The intercept at the Z' axis obtained on extrapolation of these arcs provides the tendency of the grain and grain boundary resistance for the sample before and after magnetic poling. The results suggested that the decrease of impedance was mainly due to the grain boundaries in the low frequency region. This result agrees with the viewpoint that the MI or the magneto-resistance (MR) effect of the sample is dominated by spin-polarized tunneling across grain boundaries when the sample is magnetized [29,30]. Furthermore, due to the mixed-valence nature of Mn in LBMO, there must be a double-exchange mechanism between Mn^{3+} and Mn^{4+}, which leads to the MR effects in the grains of LBMO. However, because of the small amount of LBMO and the small resistance of grains, the effects are difficult to observe in the impedance spectroscopy.

To study the mechanism of MC and ML effects, a Maxwell–Wagner (M–W) capacitor model is established, as shown in Fig. 4(d), where the black and white sections represent the LBMO and BTO grains, respectively, and the gray interface represents the grain boundaries. The real and imaginary parts of its permittivity are presented as Eqs. (3) and (4), respectively, with little differences from those in Ref. [31,32], with

the interfacial-like layer and bulk-like layer being regarded as grain boundaries and grain, respectively. The equations are

$$\varepsilon'(\omega) = \frac{1}{C_0(R_{gb}+R_g)} \frac{\tau_{gb}+\tau_g-\tau+\omega^2\tau_{gb}\tau_g\tau}{1+\omega^2\tau^2} \quad (3)$$

$$\varepsilon''(\omega) = \frac{1}{\omega C_0(R_{gb}+R_g)} \frac{1-\omega^2\tau_{gb}\tau_g+\omega^2\tau(\tau_{gb}+\tau_g)}{1+\omega^2\tau^2}, \quad (4)$$

where ω, R_g and R_{gb} refer to the same quantities as in Eqs. (1) and (2). Here, $\tau_{gb} = C_{gb}R_{gb}$, $\tau_g = C_gR_g$, $\tau = (\tau_{gb}R_g+\tau_gR_{gb})/(R_{gb}+R_g)$, $C_0 = \varepsilon_0A/t$, A is area of the capacitor, and t is thickness. In these equations, the absolute thickness is actually irrelevant; what counts instead is the thickness ratio t_{gb}/t_g. In the fine-grained ceramic with depleted grain boundaries, the value of t_{gb}/t_g is 0.1. Combined with the negative MR effects of the grain boundaries and M–W capacitor model, the negative MC effects and positive ML effects can be calculated; the results correspond to the experimental data as shown in Fig. 4(a). However, the calculation of the relationship between the MC effects and the frequency does not match the observed phenomenon. To the best of the author's knowledge, the above interpretation is preliminary and more work is required to understand the mechanism of MC coupling.

4. Conclusion

In this work, LBMO–BTO composite ceramics were prepared, and the structural, ferroelectric and ferromagnetic features and magneto-electric effects were also tested. The results indicate that the composites are multiferroic materials simultaneously exhibiting ferroelectric and ferromagnetic properties at room temperature. The composite ceramics were found to exhibit certain magneto-electronic effects. The ME effects, as represented by the *P–E* hysteresis loop measurement with and without an external uniform constant applied magnetic field, exhibited an obvious reduction of the measured remnant polarization 2Pr and coercive field 2Ec when the external magnetic field was applied. The average changes of 2Pr and 2Ec were −21.1% and −9.2%, respectively. The MC and MI negative effects were also observed, which originated from the coexistence of magnetostriction and magnetoresistance in LBMO. The composite exhibited good ME coupling at room temperature, which can be useful for potential multi-functional device applications.

Acknowledgment

The authors are grateful for financial supports from the National Natural Science Foundation of China under Grant no. 60871017 and the National High Technology Research and Development Program of China (863 Program) under Grant no. 2013AA030903.

References

[1] J.F. Scott, Multiferroic memories, Nat. Mater. 6 (2007) 256–257.
[2] M. Bibes, A. Barthélémy, Towards a magneto-electric memory, Nat. Mater. 7 (2008) 426–427.
[3] J. Ma, J.-M. Hu, Z. Li, C.-W. Nan, Recent progress in multiferroic magnetoelectric composites: from bulk to thin films, Adv. Mater. 23 (2011) 1062–1087.
[4] J.-Q. Huang, P.-Y. Du, L.-X. Hong, Y.-L. Dong, M.-C. Hong, A percolative ferromagnetic–ferroelectric composite with significant dielectric and magnetic properties, Adv. Mater. 19 (2007) 437–440.
[5] H. Zheng, Y.-L. Dong, X. Wang, W.-J. Weng, G.-R. Han, N. Ma, P.-Y. Du, Super high threshold percolative ferroelectric/ferrimagnetic composite ceramics with outstanding permittivity and initial permeability, Angew. Chem. Int. Ed. 48 (2009) 8927–8930.
[6] S.Q. Ren, L.Q. Weng, S.-H. Song, F. Li, et al., $BaTiO_3/CoFe_2O_4$ particulate composites with large high frequency magnetoelectric response, J. Mater. Sci. 40 (2005) 4375–4378.
[7] C.-X. Li, B. Yang, S.-T. Zhang, D.-Q. Liu, R. Zhang, Y. Sun, W.-W. Cao, Effects of Mn doping on multiferroic and magnetocapacitive properties of $0.33Ba_{0.70}Ca_{0.30}TiO_3$–$0.67BiFeO_3$ diphasic ceramics, J. Alloys Compd. 590 (2014) 346–354.
[8] N.G. Kim, Y.S. Koo, C.J. Won, N. Hur, J.H. Jung, J. Yoon, Y. Jo, M.H. Jung, Magnetodielectric effect in $BaTiO_3-LaMnO_3$ composites, J. Appl. Phys. 102 (2007) 014107.
[9] G. Jian, D.-X. Zhou, J.-Y. Yang, H. Shao, F. Xue, Q.-Y. Fu, Microstructure and multiferroic properties of $BaTiO_3/CoFe_2O_4$ films on Al_2O_3/Pt substrates fabricated by electrophoretic deposition, J. Eur. Ceram. Soc. 33 (2013) 1155–1163.
[10] D.-X. Zhou, G. Jian, Y.-X. Hu, Y.-N. Zheng, S.-P. Gong, H. Liu, Electrophoretic deposition of multiferroic $BaTiO_3/CoFe_2O_4$ bilayer films, Mater. Chem. Phys. 127 (2011) 316–321.
[11] Y.-J. Wu, J.-G. Wan, C.-F. Huang, Y.-Y. Weng, S.-F. Zhao, J.-M. Liu, G. hou Wang, Strong magnetoelectric coupling in multiferroic $BiFeO_3$–$Pb(Zr_{0.52}Ti_{0.48})O_3$ composite films derived from electrophoretic deposition, Appl. Phys. Lett. 93 (2008) 192915.
[12] H.-C. He, J. Ma, Y.-H. Lin, C.W. Nan, Influence of relative thickness on multiferroic properties of bilayered $Pb(Zr_{0.52}Ti_{0.48})O_3$–$CoFe_2O_4$ thin films, J. Appl. Phys. 104 (2008) 114114.
[13] H. Zheng, J. Wang, S.E. Lofland, Z. Ma, L. Mohaddes-Ardabili, T. Zhao, L. Salamanca-Riba, S.R. Shinde, S.B. Ogale, F. Bai, D. Viehland, Y. Jia, D.G. Schlom, M. Wuttig, A. Roytburd, R. Ramesh, Multiferroic $BaTiO_3$–$CoFe_2O_4$ nanostructures, Science 303 (2004) 661–663.
[14] X.-L. Lu, Y. Kim, S. Goetze, X.-G. Li, S.-N. Dong, P. Werner, M. Alexe, D. Hesse, Magnetoelectric coupling in ordered arrays of multilayered heteroepitaxial $BaTiO_3/CoFe_2O_4$ nanodots, Nano Lett. 11 (2011) 3202–3206.
[15] G. Sreenivasulu, M. Popov, F.A. Chavez, S.L. Hamilton, P.R. Lehto, G. Srinivasan, Controlled self-assembly of multiferroic core–shell nanoparticles exhibiting strong magneto-electric effects, Appl. Phys. Lett. 104 (2014) 052901.
[16] V. Corral-Flores, D. Bueno-Baqués, R.F. Ziolo, Synthesis and characterization of novel $CoFe_2O_4$–$BaTiO_3$ multiferroic core–shell-type nanostructures, Acta Mater. 58 (2010) 764–769.
[17] K. Raidongia, A. Nag, A. Sundaresan, C.N.R. Rao, Multiferroic and magnetoelectric properties of core–shell $CoFe_2O_4$@$BaTiO_3$ nanocomposites, Appl. Phys. Lett. 97 (2010) 062904.
[18] G.H. Haertling, Ferroelectric ceramics history and technology, J. Am. Ceram. Soc. 82 (1999) 797.
[19] H.L. Ju, Y.S. Nam, J.E. Lee, H.S. Shin, Anomalous magnetic properties and magnetic phase diagram of $La_{1-x}Ba_xMnO_3$, J. Magn. Magn. Mater. 219 (2000) 1–8.
[20] H.S. Im, G.B. Chon, S.M. Lee, B.H. Koo, C.G. Lee, M.H. Jung, Preparation and characterization of $La_{0.7}AE_{0.3}MnO_3$ (AE=Ca, Sr, Ba): perovskite structured manganites, J. Magn. Magn. Mater. 310 (2007) 2668–2670.
[21] R.V. Demin, L.I. Koroleva1, Y.A.M. Mukovskii, Giant volume magnetostriction and colossal magnetoresistance at room temperature in $La_{0.7}Ba_{0.3}MnO_3$, J. Phys.: Condens. Matter 17 (2005) 221–226.

[22] G. Srinivasan, E.T. Rasmussen, R. Hayes, Magnetoelectric effects in ferrite–lead zirconate titanate layered composites: the influence of zinc substitution in ferrites, Phys. Rev. B. 67 (2003) 014418.
[23] X.-Q. Chen, J. Xiao, J. Yao, Z.-W. Kang, F.-J. Yang, X.-B. Zeng, Room temperature magnetoelectric coupling study in multiferroic Bi_4NdTi_3-$Fe_{0.7}Ni_{0.3}O_{15}$ prepared by a multicalcination procedure, Ceram. Int. 40 (2014) 6815–6819.
[24] M.L. Dunn, Effects of grain shape anisotropy, porosity, and microcracks on the elastic and dielectric constants of polycrystalline piezoelectric ceramics, J. Appl. Phys. 78 (1995) 1533.
[25] Z.-M. He, J. Ma, R.-F. Zhang, Investigation on the microstructure and ferroelectric properties of porous PZT ceramics, Ceram. Int. 30 (2004) 1353–1356.
[26] T. Zeng, X.-L. Dong, C.-L. Mao, Z.-Y. Zhou, H. Yang, Effects of pore shape and porosity on the properties of porous PZT 95/5 ceramics, J. Eur. Ceram. Soc. 27 (2007) 2025–2029.
[27] N. Ortega, A. Kumar, P. Bhattacharya, S.B. Majumder, R.S. Katiyar, Impedance spectroscopy of multiferroic $PbZr_xTi_{1-x}O_3/CoFe_2O_4$ layered thin films, Phys. Rev. B 77 (2008) 014111.
[28] P. Pahuja, R. Sharma, C. Prakash, R.P. Tandon, Synthesis and characterization of $Ni_{0.8}Co_{0.2}Fe_2O_4$–$Ba_{0.95}Sr_{0.05}TiO_3$ multiferroic composites, Ceram. Int. 39 (2013) 9435–9445.
[29] H.Y. Hwang, S.-W. Cheong, N.P. Ong, B. Batlogg, Spin-polarized intergrain tunneling in $La_{2/3}Sr_{1/3}MnO_3$, Phys. Rev. Lett. 77 (1996) 2041.
[30] J. Klein, C. Häofener, S. Uhlenbruck, L. Alff, B. Bäuchner, R. Gross, On the nature of grain boundaries in the colossal magnetoresistance manganites, Europhys. Lett. 47 (1999) 371.
[31] G. Catalan, D. O'Neill, R.M. Bowman, J.M. Gregg, Relaxor features in ferroelectric superlattices: a Maxwell–Wagner approach, Appl. Phys. Lett. 77 (2000) 3078.
[32] G. Catalana, Magnetocapacitance without magnetoelectric coupling, Appl. Phys. Lett. 88 (2006) 102902.